Original article

Nuclear Medicine Communications

3D-OSEM and FP-CIT SPECT quantification: benefit for studies with a high radius of rotation?

Walter Koch, Peter Bartenstein and Christian la Fougère

Objectives **Dopamine transporter imaging with single-photon emission computed tomography (SPECT) is a valuable tool for both clinical routine and research studies. Recently, it was found that the image quality could be improved by introduction of the three-dimensional ordered subset expectation maximization (3D-OSEM) reconstruction algorithm, which provides resolution recovery. The aim of this study was to systematically evaluate the potential benefits of 3D-OSEM in comparison with 2D-OSEM under critical imaging conditions, for example, scans with a high radius of rotation.**

Materials and methods **Monte Carlo simulation scans of a digital brain phantom with various disease states and different radii of rotation ranging from 13 to 30 cm were reconstructed with both 2D-OSEM and 3D-OSEM algorithms. Specific striatal binding and putamen-to-caudate ratios were determined and compared with true values in the phantom.**

Results **The percentage recovery of true striatal binding was similar between both reconstruction algorithms at the minimum rotational radius; however, at the maximum rotational radius, it decreased from 53 to 43% for 3D-OSEM and from 52 to 26% for 2D-OSEM. 3D-OSEM matched the true putamen-to-caudate ratios more closely than did 2D-OSEM in scans with high SPECT rotation radii.**

Conclusion **3D-OSEM offers a promising image quality gain. It outperforms 2D-OSEM, particularly in studies with limited resolutions (such as scans acquired with a high radius of rotation) but does not improve the accuracy of the putamen-to-caudate ratios. Whether the benefits of better recovery in studies with higher radii of rotation could potentially increase the diagnostic power of dopamine transporter SPECT in patients with borderline striatal radiotracer binding, however, needs to be further examined.** ***Nucl Med Commun*** **34:971–977 © 2013 Wolters Kluwer Health | Lippincott Williams & Wilkins.**

Nuclear Medicine Communications 2013, **34**:971–977

Keywords: 3D-OSEM iterative reconstruction, dopamine transporter, FP-CIT, Monte Carlo simulation, radius of rotation

Department of Nuclear Medicine, University of Munich, Munich, Germany

Correspondence to Walter Koch, MD, Department of Nuclear Medicine, University of Munich, Marchioninistr 15, 81377 Munich, Germany
Tel: +49 89 7095 4646; fax: +49 89 7095 7646;
e-mail: walter.koch@med.uni-muenchen.de

Received 17 March 2013 **Revised** 21 May 2013 **Accepted** 28 June 2013

Introduction

Imaging of the presynaptic dopamine transporter (DAT) has evolved to be an important diagnostic tool in patients with Parkinsonian syndromes [1]. DAT single-photon emission computed tomography (SPECT) scans are used to confirm or exclude a neurodegenerative Parkinsonian syndrome [2] and, in combination with semiquantification [3,4], can detect subtle changes in DAT binding in striatal subregions and allow monitoring of disease progression [5,6].

Recently, the enhanced image reconstruction algorithm three-dimensional ordered subset expectation maximization (3D-OSEM) has become available for DAT imaging. The algorithm takes the depth response of the collimators into account and has been shown to provide a superior image quality in comparison with 2D-OSEM [7]. Its value for clinical routine use has been demonstrated [8]. A superiority in low-count images enables reduction of the injected radiotracer dose or the imaging time [9–11].

The potential benefits of resolution recovery (as implemented in 3D-OSEM) for semiquantitative analyses, however, have not been examined yet. An increased resolution could particularly aid in critical imaging conditions, such as performing a DAT SPECT scan with a high rotational radius, as is sometimes required because of anatomical reasons or claustrophobia. Recently, the rotation radius dependence of I-123-FP-CIT quantification was shown for 2D-OSEM reconstructions [12].

The aim of this study was to systematically evaluate the potential benefits of 3D-OSEM in comparison with 2D-OSEM for semiquantitative analyses and disease detection based on the Monte Carlo simulation of studies with various radii of rotation and different extents of Parkinson's disease.

Materials and methods

Phantom

The Zubal digital brain phantom (*http://noodle.med.yale.edu/zubal/*, G. Zubal, Yale University, New Haven, Connecticut, USA; [13]) was modified to simulate the typical profiles of the normal radiotracer binding status as well as neurodegeneration in Parkinsonian syndromes (loss of DAT binding [2]). On the basis of previous measurements with a physical phantom [14] and patient

0143-3636 © 2013 Wolters Kluwer Health | Lippincott Williams & Wilkins

DOI: 10.1097/MNM.0b013e328364a9fd

scans [15], the activity distribution within the digital phantom was chosen to reflect a realistic situation found in healthy controls and patients. For simulation of normal DAT binding, the activity concentrations of I-123 ratios between the striatal structures of each hemisphere and the remaining brain were 6 to 1 [15]. To simulate neurodegeneration, an exponential loss of DAT binding was modeled separately for the caudate and the putamen, based on τ values previously published in a long-term follow-up study on patients with idiopathic Parkinsonian syndromes [16] according to the formula: $C_s = C_0 \times exp\left(-\frac{T}{\tau}\right)$, where C_s is the activity concentration of the respective striatal region, C_0 equals the striatal concentration in a healthy state, T is the years of disease, and the τ values (reflecting the rate of disease progression) being derived from the study by Schwarz *et al.* [16].

Monte Carlo simulation

The SIMIND Monte Carlo code [17] was used to calculate projection data based on the digital brain phantom (256×256 matrix with 128 slices, $1.1 \times 1.1 \times 1.4$ mm pixel size). A dual-headed MiE ECAM variable SPECT camera (MiE, Seth, Germany) equipped with low-energy, high-resolution parallel hole collimators (parallel hexagonal holes with cells of 1.11 mm diameter, 2.405 cm height, and 0.16 mm septal thickness) was entirely modeled in the software. The comparability of the simulated data of this camera type with real equipment has been confirmed elsewhere [18]. The acquisition parameters were based on recommendations outlined in the procedure guidelines for neurotransmission SPECT with DAT ligands published by the European Association of Nuclear Medicine [3] and were applied to the Monte Carlo simulation. All acquisitions were optimized not only to obtain a high spatial resolution but also to reflect the clinical use of the SPECT systems. A total of 120 projections were obtained for each simulation, with the detector heads following a 360° circular orbit in a 128×128 matrix with a main energy window from 143.1 to 174.9 keV. In addition, a lower (131.9–143.0 keV) and an upper (175.0–186.1 keV) scatter window adjacent to the main window were acquired. The pixel size was 3.0×3.0 mm. Physical effects, such as photon attenuation and scatter in the phantom and the crystal, degradation due to collimator resolution, septal penetration, photon interaction in the collimator [19], and backscatter from the detector cover material were included in the simulations. The full energy spectrum of I-123 was simulated. Ten million counts in the main energy window were simulated for each acquired projection to obtain low noise simulation data. Study counts of the main window were then scaled to obtain total counts of 2.5 million per acquisition, as typically acquired in true patient scans. The scatter windows were consecutively scaled with identical factors. Finally, Poisson-distributed noise was added to the projection data. Apart from the original main energy window acquisitions, scatter-corrected data were calculated based on the triple energy window correction method [20,21].

Simulated disease states and radii of rotation

A healthy state ($T = 0$ years) as well as disease states 2, 4, 6, 8, and 10 years after disease onset were simulated. The simulations therefore covered a wide range, from entirely normal to preclinical as well as far-progressed disease states. Each disease state was imaged with 13, 14, 15, 16, 17, 18, 19, 20, and 30 cm radii of SPECT rotation.

SPECT processing

Simulated SPECT acquisition data were transferred to a real MiE ECAM variable camera acquisition workstation and reconstructed with a 2D-OSEM algorithm (OSEM implementation based on the algorithm of Richard Larkin from Macquarie University [22]) and with a 3D-OSEM algorithm (depth response OSEM) using the MiE Scintron software (MiE Medical Imaging Electronics, Seth, Germany). For both 2D-OSEM and 3D-OSEM reconstructions, projection data were smoothed using a two-dimensional Gaussian filter with a full-width at half-maximum of 5.65 mm. Smoothing was performed by convolution of the projection with a filter mask in each direction. The length of the filter mask is 3 with the weighting [1, 2, 1]/4. Thus, each pixel in a projection is first smoothed in the x-direction by a weighted sum including twice itself and its left and right neighbor divided by 4 in order to be count preserving. Thereafter, the procedure is repeated in the y-direction using the upper and lower neighbors of each pixel. Four iterations with 16 subsets were used to reconstruct data, and the reconstructions were corrected for attenuation ($\mu = 0.11$/cm, automated contour finding with separate contours for each slice), following Chang's method [3] for 2D-OSEM. For 3D-OSEM, attenuation correction was integrated into the reconstruction algorithm.

Automated VOI evaluation

Using shift transforms only, the digital phantom was coregistered to the reconstructed transverse slices of the 13 cm rotational radius acquisition of the healthy state. Three-dimensional volumes of interest (VOIs) for the striatal regions were defined based on digital phantom morphology (caudate or putamen). A large occipital background region was added (8624 voxels), which served as a reference for all semiquantitative analyses. The VOI sizes are given in Table 1.

Semiquantitative evaluation

Specific binding within the striatum, caudate, and putamen were calculated from the mean counts per voxel, with the occipital cortex serving as a reference [specific $\text{binding}_{\text{striatum}}$ = (striatum – occipital reference)/occipital reference]. Because the underlying disease in patients with Parkinsonian syndromes often affects the caudate nucleus and putamen with a varying severity,

Table 1 Volumes of interest used for SPECT quantification

Method of analysis	Region	Size (ml)
Morphological VOI	Striatum	6.40
	Caudate	2.39
	Putamen	4.01
Occipital reference VOI	Occipital	132.87

SPECT, single-photon emission computed tomography; VOI, volume of interest.

the putamen-to-caudate ratios (P-to-C ratios = ratio between specific putaminal and specific caudate binding) were also calculated.

Statistical analyses

Linear regression analyses were used to describe the relationship between specific binding ratios and radii of rotation. The slopes and SE of slopes were calculated.

To detect differences in the slopes of the linear regression curves, analysis of covariance was applied, investigating the significance of the interaction between the classification effect (such as the reconstruction method) and the covariate (the specific binding ratio).

To determine the influence of rotational radii on the measured binding values from a statistical point of view, multivariate general linear regression was used: true striatal binding in the phantom (as the dependent variable) was predicted on the basis of the covariates measured binding and radius of rotation. A high slope/correlation coefficient of the rotational radius therefore indicates a strong impact of this factor, whereas a low correlation coefficient indicates a weak influence.

All statistical analyses were performed using SPSS Software version 13 (SPSS Inc., Chicago, Illinois, USA). For automation of digital phantom 'filling', multithreaded Monte Carlo simulation, file format conversions, calculation of noise with Poisson distribution, DICOM packaging, data exchange with a real MiE SPECT camera, and automation of VOI quantification, an in-house software written in VB.NET 2010 (Visual Studio 2010; Microsoft Corp., Redmond, Washington, USA) was used. VOI quantification was performed using the MIPAV software (Center for Information Technology, National Institutes of Health, Bethesda, Maryland, USA). Reconstruction of the raw acquisition data sets on Scintron software was controlled by an in-house automation software based on the AutoIt scripting technology (AutoIt Consulting Ltd, Birmingham, UK, *http://www.autoitscript.com*).

The results, images, and statistics presented in text, tables, and figures are based on acquisition data without scatter correction, if not explicitly mentioned.

Results

Recovery

The measured specific striatal binding was compared with the true specific binding ratios in the phantom for both 2D-OSEM-reconstructed and 3D-OSEM-reconstructed images in the healthy state. Independent of the radius of rotation, the measured striatal binding ratios were slightly higher for 3D-OSEM images than for 2D-OSEM images. At the minimum radius of rotation (13 cm), the percentage recovery was 53% for 3D-OSEM and 52% for 2D-OSEM. At the maximum rotational radius (30 cm), the recovery decreased to 43% for 3D-OSEM and to 26% for 2D-OSEM. Addition of scatter correction increased the recovery at 13 cm to 63 and 60% and at 30 cm to 51 and 42% for 3D-OSEM and 2D-OSEM, respectively.

Radius dependency of the measured striatal binding

The correlations between specific binding ratios and radii of rotation in the healthy state for 2D-OSEM and 3D-OSEM reconstructions are shown in Fig. 1 (uncorrected data Fig. 1a, scatter-corrected data Fig. 1b). A linear loss of striatal binding with an increasing radius of rotation could be observed for both methods of reconstruction, the observation being independent of whether uncorrected or scatter-corrected data were used. For 3D-OSEM, the decrease, however, was less steep compared with that for 2D-OSEM (significantly different slopes: *F*-test $P < 0.05$), which is in line with the higher recovery values observed for 3D-OSEM in scans with larger rotational radii. Table 2 shows the results of the multivariate linear regression analyses. The results clearly demonstrate a higher influence (correlation coefficient) of the rotational radius on striatal binding in 2D-OSEM images than in 3D-OSEM images.

Figure 2 exemplarily shows images of the healthy state reconstructed with both 2D-OSEM and 3D-OSEM with different radii of rotation. 3D-OSEM images showed a better delineation of the caudate and the putamen and a smoother background (nonspecific binding) compared with 2D-OSEM images. With a higher radius, the resolution decreases, the activity spreads beyond the true borders of the striatum, and the partial-volume effects increase in all three dimensions, resulting in a loss of recovery, which is more pronounced in 2D-OSEM images. Although a horizontal, 15-mm-wide line profile through the striatal area in an acquisition with a low rotational radius shows a steep count increase from unspecific binding to striatal binding, the increase becomes shallower with an increase in the radius of rotation, with this effect being shown equally in both methods of reconstruction.

Putamen-to-caudate ratios

To estimate the potential beneficial effects of 3D-OSEM in comparison with 2D-OSEM in a clinical routine setting, we directly compared the P-to-C ratios between both methods of reconstruction as an objective parameter for determining the predominant putaminal binding loss typically observed in Parkinson's disease. Because low

Fig. 1

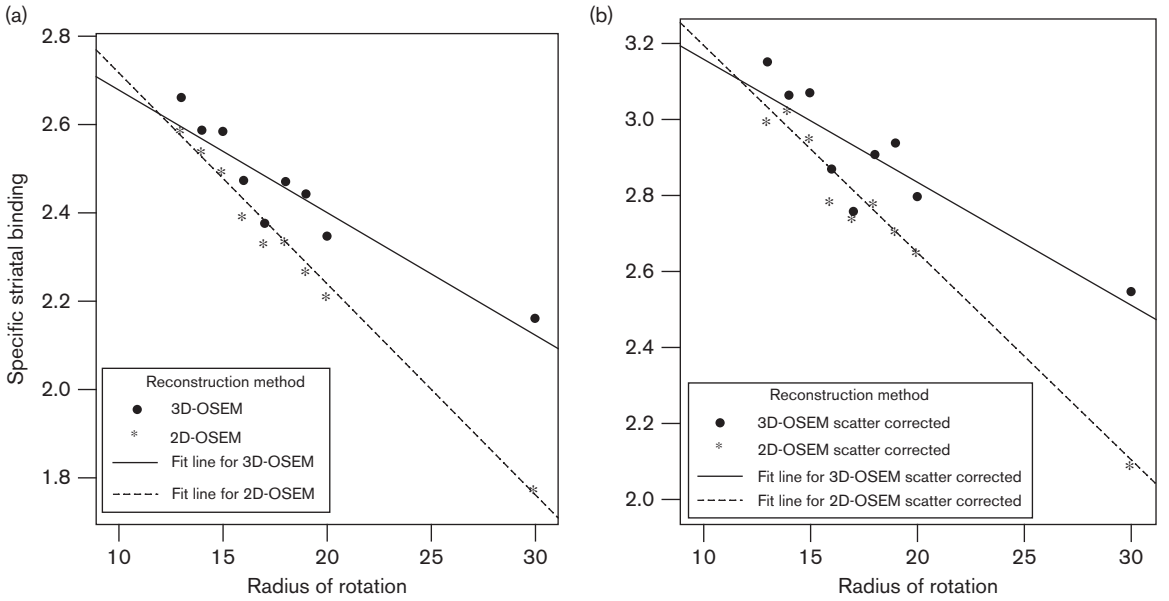

Correlations between the specific binding ratios and radii of rotation in the healthy state in 2D-OSEM-reconstructed and 3D-OSEM-reconstructed images for (a) uncorrected simulation data and (b) scatter-corrected data. OSEM, ordered subset expectation maximization.

Table 2 Relation between the radius of rotation and the measured striatal binding for 2D-OSEM and 3D-OSEM: results of the multivariate linear regression analyses

	Regression coefficient		
Method of reconstruction	Measured striatal binding±SE	Radius of rotation±SE	Constant±SE
2D-OSEM	2.146±0.026	0.320±0.004	−0.643±0.76
3D-OSEM	2.027±0.016	0.180±0.002	−0.331±0.48

OSEM, ordered subset expectation maximization.

striatal binding values result in statistical noise, these analyses were confined to a disease progression of up to a maximum of 10 years. Figure 3 exemplarily shows the correlations between the measured and true P-to-C ratios for 13 cm of rotation and 30 cm of rotation for both methods of reconstruction.

At 30 cm of rotation, the 3D-OSEM seems to outperform 2D-OSEM, with better reproduction of the true P-to-C ratios. On defining an arbitrary threshold for disease detection at a P-to-C ratio of 0.7 (30% relative loss of putaminal binding), at 13 cm of rotation, disease could be detected 3.5 years after onset using 2D-OSEM and 3D-OSEM; however, at 30 cm of rotation, the disease would have had to have progressed 5.3 years in order to be detected on 3D-OSEM images, but would have had to have progressed to at least 8.0 years for detection with 2D-OSEM reconstructions.

This presumed difference between the reconstruction methods, however, could only be observed on comparing the minimum and maximum rotational radii. Across all radii of rotation, no significant benefit of 3D-OSEM in terms of P-to-C ratio reproduction could be shown (F-test $P = 0.782$).

Discussion

Imaging of the presynaptic DAT has evolved into an important diagnostic tool for patients with Parkinsonian syndromes [1,23–25], and thus has become a routine clinical procedure. Visual assessment of DAT SPECT studies in many cases enables clinicians to decide whether neurodegeneration of presynaptic neurons has occurred and to confirm or exclude a neurodegenerative Parkinsonian syndrome [2]. In particular, for an early diagnosis, that is, the detection of subtle changes in DAT binding in striatal subregions, and for monitoring disease progression [5,6,26] or the beneficial effects of putative neuroprotective drugs [5,6,16,27,28], additional semi-quantitative measurements are essential [3].

3D-OSEM is assumed to have the potential to outperform filtered backprojection and 2D-OSEM in terms of image quality [9–11].

Fig. 2

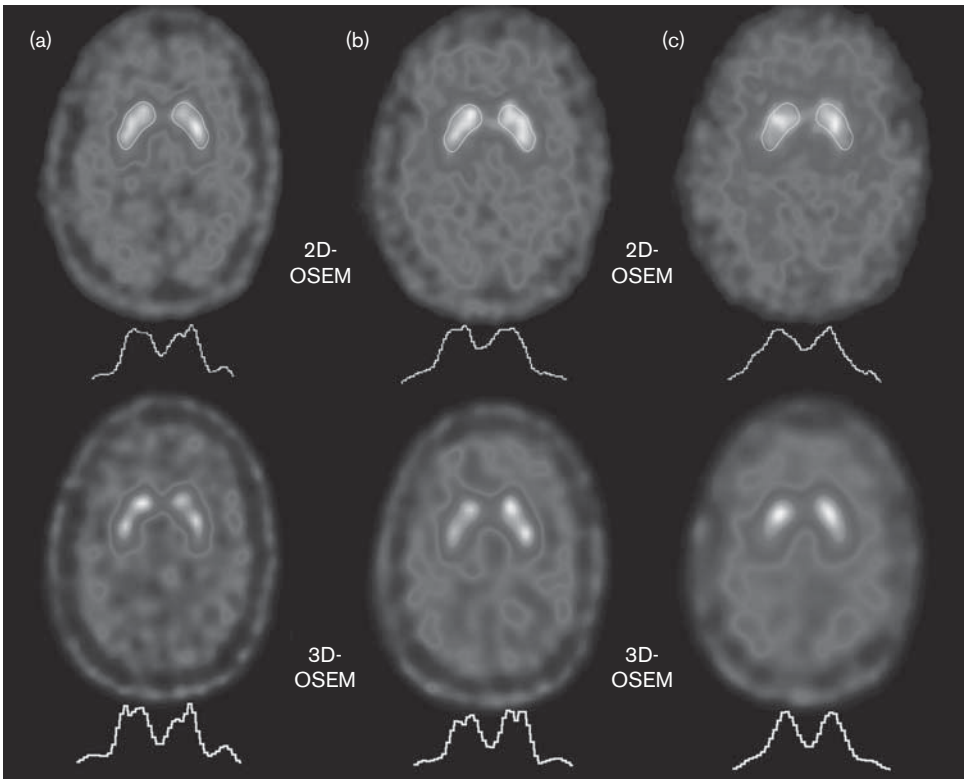

Examples for the effects of rotational radii on the image quality. Below each example, a 15 mm horizontal line profile centered on the striatal region is shown. 2D-OSEM (first row), 3D-OSEM (second row), (a) a 13 cm radius of rotation, (b) a 20 cm radius of rotation, and (c) a 30 cm radius of rotation. OSEM, ordered subset expectation maximization.

FP-CIT semiquantification shows an acquisition radius dependence that is attributed to partial-volume effects due to a drop in the resolution with increasing radius, as was recently shown by Larsson *et al.* [12]. With an increase in the full-width at half-maximum of the spatial resolution in reconstructed images, activity from within the striatum spreads over an increasing area as shown in Fig. 2, resulting in a loss of counts within the quantification VOIs (spill-out).

Radius dependence was less prominent when a three-dimensional cone beam model was incorporated in the iterative reconstruction algorithm (3D-OSEM). The resulting enhanced resolution recovery led to higher binding ratios in scans with high radii of rotation.

The difference in recovery when comparing measured and true specific striatal binding using both reconstruction methods in scans with minimal rotational radii was low (1.9%); the annual loss of DAT binding in patients with idiopathic Parkinsonian syndromes is $\sim$5.2% per year [29]. It could also be attributed to the slight differences in attenuation correction or filtering. The more prominent differences in scans with high radii of rotation (up to 19.4% at 30 cm) will most likely be related to the higher spatial resolution in 3D-OSEM images. 3D-OSEM therefore seems more robust to the influence of the radius of rotation. The overall measured binding values based on uncorrected data were in a typical range of about half the true activity ratios in the phantom, which can be attributed mainly to scatter and partial-volume effects. Scatter correction led to a general increase in recovery, in studies with both low and high radii of rotation, but did not have an effect on the radius dependence of the binding values. Scatter correction, however, is typically not applied in a routine setting. If further reduction of partial-volume effects is required, the 'Southampton' semiquantification method proposed by Fleming and colleagues [30,31] would provide a promising method to overcome the influence of rotational radius effects.

We would have expected that an increased spatial resolution also has beneficial effects on the accuracy of the P-to-C ratios. Parkinson's disease typically affects the putamen earlier, given the more prominent nigrostriatal degeneration in that region [32,33] and the particular degeneration of the ventrolateral substantia nigra pars compacta [34], which innervates the posterior putamen [35]. P-to-C ratios therefore offer diagnostic information, independent of total specific striatal binding [36].

Fig. 3

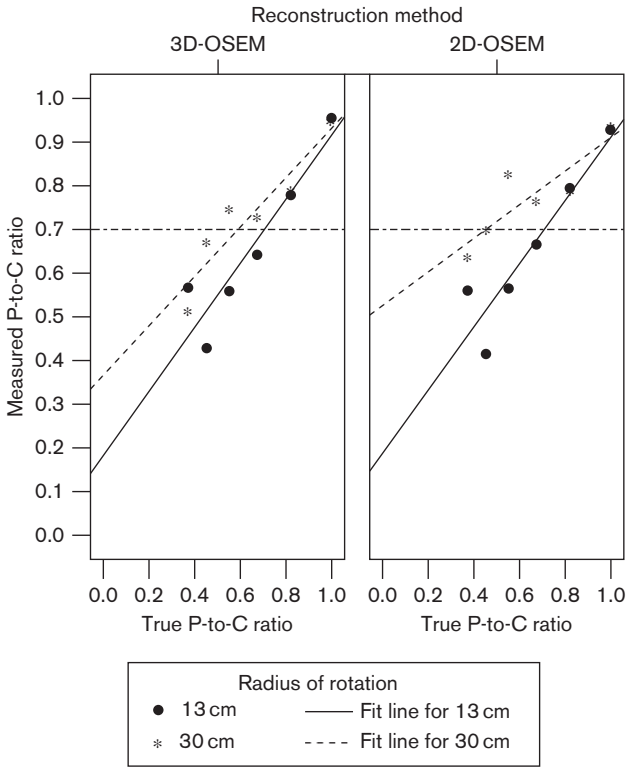

Correlations between the measured and true P-to-C ratios in scans with a 13 cm radius of rotation and a 30 cm of rotation for both 2D-OSEM and 3D-OSEM reconstructions. The horizontal line represents an arbitrary threshold for differentiation of pathological and normal scan results. Both healthy and disease states are represented. OSEM, ordered subset expectation maximization; P-to-C ratios, putamen-to-caudate ratio.

With a higher spatial resolution, we assumed an earlier (in terms of disease progression) decrease in the P-to-C ratios, as the activity spread from the caudate to the putamen due to partial-volume effects would be less. This could in fact be shown when comparing scans with minimum (13 cm) and maximum (30 cm) radii of rotation; however, the effect did not reach the level of significance and could not be shown for scans with less extreme rotational radii (for e.g. 20 cm). At least in terms of P-to-C ratios as diagnostic markers, an improved image quality of 3D-OSEM, as described by Winz *et al.* [8], did not yield a diagnostic benefit.

The decision whether an individual patient scan is normal or pathological is, however, based upon the comparison of the measured striatal binding values with (ideally age-matched) reference values rather than on P-to-C ratios alone [3,4,15]. On the basis of this approach, underestimation of specific striatal binding in 2D-OSEM-reconstructed scans with high radii of rotation could therefore result in misclassification of a healthy patient as diseased. In theory, the diagnostic power for patients with borderline DAT binding could therefore be increased by applying 3D-OSEM. Whether 3D-OSEM could lead to a significant gain in diagnostic power, however, would need further evaluation in patient studies.

Some limitations of our results should be acknowledged. Our data were obtained under ideal conditions, without movement artefacts and with standardized reorientation and symmetrical activity concentrations in the phantom in both hemispheres. Often patients with idiopathic or nonidiopathic Parkinsonian syndromes show an asymmetric radiotracer uptake. The activity spread with increasing rotational radii could result in some spill-over of the striatal activity to the contralateral side. Apart from the rotation radius effects described here, asymmetric binding could theoretically lead to an uncorrectable overestimation of the binding in the striatum with a lower tracer update and *vice versa*.

We decided to use the Monte Carlo simulation because of the limitations resulting from the construction of conventional physical phantoms: physical phantoms cannot resemble the true anatomy as closely as can digital phantoms. Multiple acquisitions of the same patient using different spatial resolutions (radii of rotation) also seems unfeasible, as the radiotracer equilibrium time window for scanning is limited [37] and confounding factors such as patient movement during acquisition [38] or misalignment/observer-dependence of quantification [39] need to be additionally considered.

Conclusion

3D-OSEM offers promising image quality gain. It outperforms 2D-OSEM, particularly in studies with limited resolutions (such as scans acquired with a high radius of rotation) but does not improve the accuracy of the P-to-C ratios. Whether the benefits of better recovery in studies with higher radii rotation could potentially increase the diagnostic power of DAT SPECT in patients with borderline striatal radiotracer binding, however, needs to be further examined.

Acknowledgements

The authors thank Dr rer. nat. Dipl.-Inf. Hanno Schumacher (MiE Germany) for providing insights in the MiE implementation of 2D-OSEM and 3D-OSEM reconstruction and filtering as well as providing information on how to transfer the Monte Carlo simulation data to the gamma camera system.

Conflicts of interest

There are no conflicts of interest.

References

1 Booij J, Speelman JD, Horstink MW, Wolters EC. The clinical benefit of imaging striatal dopamine transporters with [^{123}I]FP-CIT SPET in

differentiating patients with presynaptic parkinsonism from those with other forms of parkinsonism. *Eur J Nucl Med* 2001; **28**:266–272.
2 Benamer TS, Patterson J, Grosset DG, Booij J, de Bruin K, van Royen E, *et al*. Accurate differentiation of parkinsonism and essential tremor using visual assessment of [^{123}I]-FP-CIT SPECT imaging: the [^{123}I]-FP-CIT study group. *Mov Disord* 2000; **15**:503–510.
3 Tatsch K, Asenbaum S, Bartenstein P, Catafau A, Halldin C, Pilowsky LS, *et al*. European Association of Nuclear Medicine procedure guidelines for brain neurotransmission SPECT using (123)I-labelled dopamine D(2) transporter ligands. *Eur J Nucl Med Mol Imaging* 2002; **29**:BP30–BP35.
4 Nobili F, Naseri M, De Carli F, Asenbaum S, Booij J, Darcourt J, *et al*. Automatic semi-quantification of [(123)I]FP-CIT SPECT scans in healthy volunteers using BasGan version 2: results from the ENC-DAT database. *Eur J Nucl Med Mol Imaging* 2013; **40**:565–573.
5 Chouker M, Tatsch K, Linke R, Pogarell O, Hahn K, Schwarz J. Striatal dopamine transporter binding in early to moderately advanced parkinson's disease: monitoring of disease progression over 2 years. *Nucl Med Commun* 2001; **22**:721–725.
6 Pirker W, Djamshidian S, Asenbaum S, Gerschlager W, Tribl G, Hoffmann M, *et al*. Progression of dopaminergic degeneration in parkinson's disease and atypical parkinsonism: a longitudinal beta-CIT SPECT study. *Mov Disord* 2002; **17**:45–53.
7 Romer W, Reichel N, Vija HA, Nickel I, Hornegger J, Bautz W, *et al*. Isotropic reconstruction of SPECT data using OSEM3D: correlation with CT. *Acad Radiol* 2006; **13**:496–502.
8 Winz OH, Hellwig S, Mix M, Weber WA, Mottaghy FM, Schafer WM, *et al*. Image quality and data quantification in dopamine transporter SPECT: advantage of 3-dimensional OSEM reconstruction? *Clin Nucl Med* 2012; **37**:866–871.
9 Alzimami KS, Sassi SA, Alkhorayef MA, Spyrou NM. Preliminary Monte Carlo study of (18)F-FDG SPECT imaging with LaBr(3): Ce crystal-based gamma cameras. Conference proceedings: Annual International Conference of the IEEE Engineering in Medicine and Biology Society, IEEE Engineering in Medicine and Biology Society Conference; 31 August to 4 September 2010, Buenos Aires Sheraton Hotel, Buenos Aires, Argentina; pp. 3089–3092.
10 Sheehy N, Tetrault TA, Zurakowski D, Vija AH, Fahey FH, Treves ST. Pediatric ^{99m}Tc-DMSA SPECT performed by using iterative reconstruction with isotropic resolution recovery: improved image quality and reduced radiopharmaceutical activity. *Radiology* 2009; **251**:511–516.
11 Stansfield EC, Sheehy N, Zurakowski D, Vija AH, Fahey FH, Treves ST. Pediatric ^{99m}Tc-MDP bone SPECT with ordered subset expectation maximization iterative reconstruction with isotropic 3D resolution recovery. *Radiology* 2010; **257**:793–801.
12 Larsson A, Mo SJ, Riklund K. Rotation radius dependence of ^{123}I-FP-CIT and ^{123}I-IBZM SPECT uptake ratios: a Monte Carlo study. *J Nucl Med Technol* 2012; **40**:249–254.
13 Zubal IG, Harrell CR, Smith EO, Rattner Z, Gindi G, Hoffer PB. Computerized 3-dimensional segmented human anatomy. *Med Phys* 1994; **21**:299–302.
14 Koch W, Radau PE, Munzing W, Tatsch K. Cross-camera comparison of SPECT measurements of a 3-D anthropomorphic basal ganglia phantom. *Eur J Nucl Med Mol Imaging* 2006; **33**:495–502.
15 Koch W, Hornung J, Hamann C, Popperl G, Tatsch K. Equipment-independent reference values for dopamine transporter imaging with ^{123}I-FP-CIT. *Nuklearmedizin* 2007; **46**:107–111.
16 Schwarz J, Storch A, Koch W, Pogarell O, Radau PE, Tatsch K. Loss of dopamine transporter binding in Parkinson's disease follows a single exponential rather than linear decline. *J Nucl Med* 2004; **45**:1694–1697.
17 Ljungberg M. The SIMIND Monte Carlo program. In: Ljungberg M, Strand S-E, King MA, editors. *Monte Carlo calculation in nuclear medicine: applications in diagnostic imaging*. Bristol and Philadelphia: IOP Publishing; 1998. pp. 145–163.
18 Bahreyni Toossi MT, Islamian JP, Momennezhad M, Ljungberg M, Naseri SH. SIMIND Monte Carlo simulation of a single photon emission CT. *J Med Phys* 2010; **35**:42–47.
19 Ljungberg M, Larsson A, Johansson L. A new collimator simulation in SIMIND based on the delta-scattering technique. *IEEE Trans Nucl Sci* 2005; **52**:1370–1375.
20 Lagerburg V, de Nijs R, Holm S, Svarer C. A comparison of different energy window subtraction methods to correct for scatter and downscatter in I-123 SPECT imaging. *Nucl Med Commun* 2012; **33**:708–718.
21 Ogawa K, Harata Y, Ichihara T, Kubo A, Hashimoto S. A practical method for position dependent Compton scatter correction in single photon emission CT. *IEEE Trans Med Imaging* 1991; **10**:408–412.
22 Hudson H, Larkin R. Accelerated image reconstruction using ordered subsets of projection data. *IEEE Trans Med Imaging* 1994; **13**:594–600.
23 Oertel WH, Gerstner A, Hoffken H, Dodel RC, Eggert KM, Moller JC. Role of dopamine transporter SPECT for the practitioner and the general neurologist. *Mov Disord* 2003; **18 (Suppl 7)**:S9–S15.
24 Poewe W, Scherfler C. Role of dopamine transporter imaging in investigation of parkinsonian syndromes in routine clinical practice. *Mov Disord* 2003; **18 (Suppl 7)**:S16–S21.
25 Marshall V, Grosset DG. Role of dopamine transporter imaging in the diagnosis of atypical tremor disorders. *Mov Disord* 2003; **18 (Suppl 7)**: S22–S27.
26 Staffen W, Mair A, Unterrainer J, Trinka E, Ladurner G. Measuring the progression of idiopathic parkinson's disease with [^{123}I] beta-CIT SPECT. *J Neural Transm* 2000; **107**:543–552.
27 Parkinson Study Group. Dopamine transporter brain imaging to assess the effects of pramipexole vs levodopa on Parkinson disease progression. *JAMA* 2002; **287**:1653–1661.
28 Pirker W, Holler I, Gerschlager W, Asenbaum S, Zettinig G, Brucke T. Measuring the rate of progression of Parkinson's disease over a 5-year period with beta-CIT SPECT. *Mov Disord* 2003; **18**:1266–1272.
29 Group PS. Dopamine transporter brain imaging to assess the effects of pramipexole vs levodopa on Parkinson disease progression. *JAMA* 2002; **287**:1653–1661.
30 Fleming JS, Bolt L, Stratford JS, Kemp PM. The specific uptake size index for quantifying radiopharmaceutical uptake. *Phys Med Biol* 2004; **49**: N227–N234.
31 Tossici-Bolt L, Hoffmann SM, Kemp PM, Mehta RL, Fleming JS. Quantification of [(123)I]FP-CIT SPECT brain images: an accurate technique for measurement of the specific binding ratio. *Eur J Nucl Med Mol Imaging* 2006; **33**:1491–1499.
32 Kish SJ, Shannak K, Hornykiewicz O. Uneven pattern of dopamine loss in the striatum of patients with idiopathic Parkinson's disease. Pathophysiologic and clinical implications. *N Engl J Med* 1988; **318**:876–880.
33 Jokinen P, Helenius H, Rauhala E, Bruck A, Eskola O, Rinne JO. Simple ratio analysis of ^{18}F-fluorodopa uptake in striatal subregions separates patients with early Parkinson disease from healthy controls. *J Nucl Med* 2009; **50**:893–899.
34 Damier P, Hirsch EC, Agid Y, Graybiel AM. The substantia nigra of the human brain. II. Patterns of loss of dopamine-containing neurons in Parkinson's disease. *Brain* 1999; **122**:1437–1448.
35 Fearnley JM, Lees AJ. Ageing and Parkinson's disease: substantia nigra regional selectivity. *Brain* 1991; **114**:2283–2301.
36 Koch W, Hamann C, Radau PE, Tatsch K. Does combined imaging of the pre- and postsynaptic dopaminergic system increase the diagnostic accuracy in the differential diagnosis of parkinsonism? *Eur J Nucl Med Mol Imaging* 2007; **34**:1265–1273.
37 Seibyl JP, Marek K, Sheff K, Zoghbi S, Baldwin RM, Charney DS, *et al*. Iodine-123-beta-CIT and iodine-123-FPCIT SPECT measurement of dopamine transporters in healthy subjects and Parkinson's patients. *J Nucl Med* 1998; **39**:1500–1508.
38 Koch W, Mustafa M, Zach C, Tatsch K. Influence of movement on FP-CIT SPECT quantification: a Monte Carlo based simulation. *Nucl Med Commun* 2007; **28**:603–614.
39 Koch W, Radau PE, Hamann C, Tatsch K. Clinical testing of an optimized software solution for an automated, observer-independent evaluation of dopamine transporter SPECT studies. *J Nucl Med* 2005; **46**: 1109–1118.